28th Annual Workshop on
Mathematical Problems in Industry
University of Delaware, June 11–15, 2012

Modeling industrial coalescers: droplet dynamics

"Droplet stability and coalescence" problem presented by
Dr. Mark Hurwitz
Pall Corporation

Participants:

D. Ambrose	Z. Di	I. Seríc
M. Arellano	P. Dubowski	B. Tilley
D. Badamor	A. Mitrano	D. Torrejon
J. Barden	M. Panaggio	S. Whitney
C. Brett	J. Pelesko	T. Witelski
F. Chen	E. Sabo	L. Yu
I. Christov	W. Sanguinet	

Summary Presentation given by I. Christov, E. Sabo, W. Sanguinet (6/15/12)
Summary Report compiled by Burt Tilley and Tom Witelski

---

1 Introduction

Filtration and separation of a mixture of different fluid components are fundamental in a wide variety of applications. These processes are used in the purification of water, for example, along with the development of chemical reactors for food processing and other biological applications. Intrinsic in these systems is the goal to remove contaminants or other fluid components from one fluid, or to harness a component in a mixture for later use. The physical mechanisms of advection and diffusion of a fluid mixture act to prevent segregation of components in general, so other physical phenomena need to be utilized to counter mixing.

However, when the fluid components of the mixture are immiscible, diffusion of one species into the second is slow compared to the advective time scale of the fluid mixture. In this situation, fluid drops of one species deform and migrate, and the dynamics of the drop within the base flow can act toward coalescence, where smaller drops merge to form fewer, larger drops, or disperse and become finer. The drop dynamics depends on the surface tension between the two fluids, assuming evaporation and condensation effects are negligible. Further, as capillary effects become more significant, changes pressure fluctuations along the flow path can become sharp, leading to reduced performance in the condensers, or even equipment damage.

The fundamental study of liquid drop dynamics in a gas has been of interest for many years. A phenomenological mapping of the different outcomes of the collision of two liquid drops was perfomed by Qian and Law [21]. In these experiments, using water drops initially and comparing the results for hydrocarbon liquids, they found that several outcomes are possible. The drops can coalesce and form a larger, single drop. The drops can bounce off of each other, or the drops

can merge initially, but then rupture into multiple drops, or fragmentation. The parameters that lead to a map of these dynamics is the Weber number and the angle made between the velocity vector and the line segement connecting the drops' centers of mass. However, the boundaries that determine the transitions in outcomes depends on the density of the surrounding gas. Further, they found that coalescence is enhanced when the vapor pressure of the liquid in the gas is larger.

Another context in which fragmentation occurs is in understanding the dynamics of raindrops during descent. The terminal velocity of the drop depends on the weight of the drop, capillarity, and inertial drag. However, if the drop is sufficiently large, then capillary forces are weaker, leading the drop to flatten, and spread, much like a parachute, and the shape develops a capillary rim along the flattened edge. This rim ruptures and becomes unstable due to the classical Raleigh criterion, with the resulting process called fragmentation [26]. The resulting drops do not coalesce during their descent, and their velocities are significantly reduced compared to the initial drop velocity [27].

In the workshop, the group worked in on two different length scales. One group consider the case when the cylindrical condensor size is much larger than the drop size. The condensor radius is assumed to be much smaller than the condensor length. Here, the mixture of drops and gas was assumed to be an effective compressible fluid medium. In the case when the Reynolds number is small, then the steady-state pressure and concentration distribution depends on the steady density distribution. However, the steady density distribution depends on the number density of specific drop sizes. One approach used here assumes that the specific volume of the mixture is a linear fit of the specific volume of the fluid and of the gas. If the gas is incompressible, then a classical linear pressure gradient is found, and a uniform distribution of liquid concentration. The state equation again plays a role in the modeling of the case for large Reynolds number. In this case, the leading-order equations result in a hyperbolic system of equations for the effective density, liquid concentration and velocity. This work is described in Section 2.

A second group consider whether a single drop, impacting a cylindrical fiber, would remain attached to the fiber. In their approach, a single differential equation for the velocity of the drop's center of mass *after impact* is found, which depends on the ratio of the initial drop's radius to the fiber, as well as the capillary length scale of the drop. For a single drop the model suggests a critical drop radius below which the drop attaches for a prescribed gas velocity. The group then considered a simulation of a distribution of different drop sizes, and the rate of filtration of the drops depends on the size distribution of the drops. This work is described in Section 3. We discuss future work of these different approaches in Section 4.

2 Large-scale models

In this section, we consider modeling the condensing process within the condensor in the case when the length scale transverse to the average flow is small compared to the length scale in the direction of the average flow. Consider the case shown in Figure 1. An initial mixture of small drops of liquid in gas is pumped into a cylinder of radius R, and we are interested in the concentration of a mixture of large and small drops at the end of the condensor $z^* = L \gg R$. For simplicity, we assume that there are at most two drop sizes, r_1, r_2 that can occur in this system, each with volumetric concentrations C_1 and C_2, respectively, with net concentration $c = c_1 + 2\,c_2$. We are interested in two different operational situations: slow-flow situations when inertial effects in the gas phase are small; and high volumetric flow rates when viscous effects are negligible. Note that

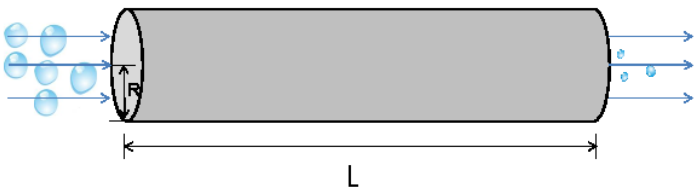

Figure 1: Inlet pipe cartoon of condenser, assuming no drop adhesion to the pipe walls, and only two drop sizes that evolve through a reversible reaction

the resulting models are restricted in the physical situations under which they apply, but they give some insight into the behavior that can be observed during operation.

The first significant modeling assumption is that we can model the mixture of air, small drops, and large drops as an effective fluid mixture. Note that this assumption requires that surface tension effects are considered negligible $We \gg 1$, since any capillary pressures would be expected to impact the momentum of the net mixture.

Although the individual phases of the gas and the liquid may be incompressible, the effective density of the mixture depends on the local volumetric concentrations of the small and large drops, and hence the mixture is a compressible fluid. With that, we assume that the mixture is an isothermal compressible fluid and its mass and momentum conservation are given by

$$\frac{\partial \rho^*}{\partial t^*} + \nabla^* \cdot (\rho^* \, \vec{\mathbf{u}}^*) = 0 \ , \tag{1}$$

$$\rho^* \frac{D\vec{\mathbf{u}}^*}{Dt^*} = -\nabla^* p^* + \mu \left\{ \nabla^{*2} \, \vec{\mathbf{u}} + \frac{1}{3} \nabla^* \left(\nabla^* \cdot \vec{\mathbf{u}}^* \right) \right\} \ , \tag{2}$$

where ρ^* is the density of the fluid mixture, which depends on the local gas concentration c, and the densities of the fluid and the gas, $\vec{\mathbf{u}}^* = u^* \mathbf{r} + w^* \mathbf{z}$ is the velocity of the fluid mixture, p^* is the mixture pressure, μ is the viscosity of the mixture, which for simplicity here is assumed constant, and D/Dt^* is the material derivative. The modeling proposed here is analogous to classical continuum modeling approaches (see [14] for a review). In these models, a constituitive equation is required for both the mixture density ρ^* and mixture pressure p^*.

Lastly, we need to describe the evolution of the drop concentration c. We assume that the drop concentration is conserved

$$\frac{\partial c}{\partial t^*} + \nabla^* \cdot (c \vec{\mathbf{u}}^*) = 0 \ . \tag{3}$$

Note that the mass and momentum equations (1), (2) require symmetry conditions along $r^* = 0$

$$\underline{r^* = 0}: \quad \lim_{r^* \to 0} r^* \frac{\partial w^*}{\partial r^*} = 0 \ , \ u^* = 0 \ , \tag{4}$$

along with the no-slip and no penetration boundary conditions along the cylinder wall

$$\underline{r^* = R}: \quad w^* = u^* = 0 \ . \tag{5}$$

For the pressure, we prescribe a pressure drop over the axial length of the cylinder

$$z^* = 0: \qquad p^* = \Delta P + P_a \ , \tag{6}$$

$$z^* = L: \qquad p^* = P_a \ , \tag{7}$$

where P_a is the ambient gas pressure, and ΔP is the applied pressure differential.

Lastly, for boundary conditions for c, we prescribe an initial distribution of the drop concentrations c at $t^* = 0$, and that the radial flux of the bubble concentration vanishes at $r^* = 0$ and at $r^* = R$,

$$z^* = 0: \qquad c = c_o(r^*, t^*) \ , \tag{8}$$

$$r^* = 0: \qquad \lim_{r^* \to 0} r^* \frac{\partial c}{\partial r^*} = 0 \ , \tag{9}$$

$$r^* = R: \qquad \frac{\partial c}{\partial r^*} = 0 \ . \tag{10}$$

We scale the radial coordinate r^* on R, the axial coordinate z^* on L, the axial velocity w^* on a scale W, the radial velocity u^* on RW/L, the time t^* on L/W, and lastly the pressure is defined as

$$p^* = P_a + (\Delta P)\, p(r, z, t) \ ,$$

where r, z, t are the dimensionless versions of the spatial coordinates and time, respectively. If we set $W = R^2(\Delta P)/(\mu L)$, or using the viscous velocity scale, the dimensionless versions of (1)-(2) and (3) become

$$\frac{\partial \rho}{\partial t} + \nabla \cdot (\rho\, \vec{\mathbf{u}}) = 0 \ , \tag{11}$$

$$\epsilon^2 \rho\, Re \frac{Du}{Dt} = -\frac{1}{\epsilon}\frac{\partial p}{\partial r} + \epsilon \left\{ \frac{1}{r}\frac{\partial}{\partial r}\left(r \frac{\partial u}{\partial r} \right) - \frac{u}{r^2} + \epsilon^2 \frac{\partial^2 u}{\partial z^2} + \frac{1}{3}\frac{\partial}{\partial r}\left(\nabla \cdot \vec{\mathbf{u}} \right) \right\} \ , \tag{12}$$

$$\epsilon \rho\, Re \frac{Dw}{Dt} = -\frac{\partial p}{\partial z} + \left\{ \frac{1}{r}\frac{\partial}{\partial r}\left(r \frac{\partial w}{\partial r} \right) + \epsilon^2 \frac{\partial^2 w}{\partial z^2} + \frac{\epsilon}{3} \nabla \left(\nabla \cdot \vec{\mathbf{u}} \right) \right\} \ , \tag{13}$$

$$\frac{\partial c}{\partial t} + \nabla \cdot (c \vec{\mathbf{u}}) = 0 \tag{14}$$

where $\epsilon = R/L$ is the aspect ratio of the condensor, ρ_a is the reference density of the mixture, and $Re = \rho_a RW/\mu$ is the Reynolds number of the mixture.

2.1 $Re \ll 1$

If we consider the $Re \ll 1$ limit, we ignore the inertial terms in (12) and (13), and expand the unknowns ρ, c_1, c_2, u, w, p in a regular asymptotic series in ϵ. For clarity in the presentation, we consider on the leading-order terms for each of the unknowns.

From (13), the leading-order equation for the pressure is given by

$$\frac{\partial p_o}{\partial r} = 0 \ ,$$

which gives that $p_o(r, z, t) = p_o(z, t)$. Note that from an equation of state, this then implies that $\rho_o = \rho_o(z, t)$. Similarly, the leading-order axial momentum equation is given by

$$\frac{1}{r}\frac{\partial}{\partial r}\left(r \frac{\partial w_o}{\partial r} \right) = 0 \ ,$$

subject to the boundary condition

$$\lim_{r\to 0} r\frac{\partial w_o}{\partial r} = 0 \ , \ w_o(1,z,t) = 0 \ ,$$

which results in a solution in terms of p_o

$$w_o = \frac{\partial p_o}{\partial z}\left(\frac{r^2-1}{4}\right) \ . \tag{15}$$

Formally, p_o and ρ_o are related by a state equation, which depends on the bubble concentration c. To close the relations between the density and the pressure, we solve for the radial velocity u using the mass conservation equation (11)

$$\frac{1}{r}\left(ru_o\right)_r \ = \ -\frac{\rho_{ot}}{\rho_o} - \frac{1}{\rho_o}\left(\rho_o p_{oz}\right)_z\left(\frac{r^2-1}{4}\right) \ . \tag{16}$$

Integrating (16) with respect to r and prescribing both $u_o = 0$ along $r = 0$ and $r = 1$ results in the following relation between the pressure and the density

$$\frac{\partial \rho_o}{\partial t} = \frac{1}{8}\frac{\partial}{\partial z}\left\{\rho_o \frac{\partial p_o}{\partial z}\right\}_z \ . \tag{17}$$

If we integrate the leading-order drop concentration equation (14) over the cross-section, we find that

$$\frac{1}{2}\frac{\partial \bar{c}}{\partial t} + \frac{\partial}{\partial z}\left\{\int_0^1 c\, w_o\, r\, dr\right\} = 0 \ , \tag{18}$$

where $\bar{c}$ is the cross-sectional average of the drop concentration. For simplicity, we assume that $c(r,z,t) = \bar{c}(z,t)$ and arrive a the following advection equation for $\bar{c}$

$$\frac{\partial \bar{c}}{\partial t} - \frac{1}{8}\frac{\partial}{\partial z}\left\{\bar{c}\,\frac{\partial p_o}{\partial z}\right\} = 0 \ , \tag{19}$$

Hence, we need one additional equation to relate the mixture density ρ_o, the pressure p_o, and the local drop concentration $\bar{c}$ to close the system. However, we can formally solve for $(p_o, \bar{c}) = (P_s(z), C_s(z))$, the steady-state solutions of (17), (19) in terms of the steady density distribution $\rho_s(z)$, subject to the boundary conditions

$$\underline{z=0}: \ p_o = 1 \ , \ \bar{c} = c_o \ \ \underline{z=1}: \ p_o = 0 \ .$$

We find that

$$P_s = \frac{\int_z^1 1/\rho_s \, d\bar{z}}{\int_0^1 1/\rho_s \, d\bar{z}} \ , \ C_s = c_0\,\frac{\rho_s(z)}{\rho_s(0)} \ . \tag{20}$$

2.2 Quasi-incompressibility

These continuum models require assumptions on the mixture pressure and the mixture density. One approach that was considered at the Workshop centered on using quasi-incompressibility, which

introduced by Joseph[13] . Suppose we require that the specific volume of the mixture follows the standard mixture rule

$$\frac{1}{\rho} = \frac{1-c}{\alpha} + c \ , \tag{21}$$

where we assume the gas density $\alpha = \rho_1/\rho_2$ is constant. Note that if each phase (gas and droplet) is isothermal, then this relation suggests that the gas and droplet pressures are equivalent. If we take the material derivative of both sides if (21), then we find

$$\begin{aligned} \frac{D}{Dt}\left(\frac{1}{\rho}\right) &= -\frac{1}{\rho^2}\frac{D\rho}{Dt} \\ &= \left(1-\frac{1}{\alpha}\right)\frac{Dc}{Dt} \\ &= \left(\frac{1}{\alpha}-1\right)(\nabla\cdot\vec{\mathbf{u}})\ c \\ &= \frac{1}{\rho^2}\,\rho\nabla\cdot\vec{\mathbf{u}} \ , \end{aligned} \tag{22}$$

which, along with (21) requires that $\nabla\cdot\vec{\mathbf{u}} = 0$. Using our asymptotic approach above, (17) becomes

$$\frac{\partial^2 p_o}{\partial z^2} = 0 \ .$$

Thus, the dynamics of the drop concentration follows an advection-diffusion equation.

$$\frac{\partial \bar{c}}{\partial t} - \frac{1}{8}\frac{\partial \bar{c}}{\partial z} = 0 \ ,$$

subject to the initial data $c(z,0) = g(z)$ and $c_(0,t) = c_o$. The transient solution is given by

$$\bar{c}(z,t) = \begin{cases} c_o & z < \frac{t}{8} \\ g(z+t/8) & z > \frac{t}{8} \end{cases} \ ,$$

Note that in steady state, ρ approaches a constant value determined by its value at $z = 0$, and (20) recovers the steady state

Formally, we can also consider in this limit the case when the gas phase is compressible. If we allow $\alpha = \alpha(z,t)$, then we can re-write the Reynolds equation (17) in terms of the dynamic equation for α in terms of the pressure p_o

$$\frac{\partial \alpha}{\partial t} = \frac{1}{8}\left\{\frac{\alpha}{1-c}\frac{\partial^2 p_o}{\partial z^2} + \frac{\partial \alpha}{\partial z}\,\frac{\partial p_o}{\partial z}\right\} \ , \ . \tag{23}$$

having used the quasi-incompressiblity relation (21). We still need an additional state equation for α, and if we use the traditional ideal gas law, nondimensionalized as

$$\alpha = \alpha_o\left(1 + M^2 p_o\right) \ ,$$

where M is the Mach number of the flow, then the coupled system of equations for $\bar{c}, p_o$ can be written as

$$M^2\frac{\partial p_o}{\partial t} = \frac{1}{8}\left[\frac{1+M^2}{1-c}\frac{\partial^2 p_o}{\partial z^2} + M^2\left(\frac{\partial p_o}{\partial z}\right)^2\right] \ , \tag{24}$$

$$\frac{\partial \bar{c}}{\partial t} = \frac{1}{8}\frac{\partial}{\partial z}\left[\bar{c}\frac{\partial p_o}{\partial z}\right] \ . \tag{25}$$

Note that as $M \to 0$, we recover the incompressible case described above.

2.2.1 Simple drop dynamics modeling

During the workshop, we considered a simple conceptual case when there are only two drop sizes, with respective drop concentrations c_1 and c_2. With this assumption, we find that $\bar{c} = c_1 + 2c_2$, and provided that there are no sources of condensed liquid entering the system, then we can write the state equations as

$$\frac{\partial c_1}{\partial t} = \frac{1}{8}\frac{\partial}{\partial z}\left[c_1 \frac{\partial p_o}{\partial z}\right] + 2\,\mathcal{R}(c_1, c_2)\ , \tag{26}$$

$$\frac{\partial c_2}{\partial t} = \frac{1}{8}\frac{\partial}{\partial z}\left[c_2 \frac{\partial p_o}{\partial z}\right] - \mathcal{R}(c_1, c_2)\ , \tag{27}$$

where $\mathcal{R}$ is a reaction term that models the reaction of smaller drops coalescing into a larger drop, or larger drops separating into smaller drops. A simple reaction model was proposed

$$\mathcal{R}(c_1, c_2) = \beta\left(kc_2 - c_1^2\right)\ ,$$

where β is a ratio of the advective time scale to the time scale of coalescense. The parameter k provides the equilibrium balance between the concentrations of the smaller and larger drops.

2.3 $Re \gg 1$

The second limit we consider is the large Reynolds number case, where viscous effects are negligible. In this limit, we allow for the gas to be compressible, and for the liquid to be incompressible. These assumptions leads to the local gas density, α, to be an unknown to be determined in the equations. We scale (1), (2) now on the characteristic velocity $W = \sqrt{P_o/\rho_2}$, where ρ_o is the ambient mixture density, pressures on the ambient reference pressure P_o, time on L/W, and density on the reference mixture density ρ_2, to find the system (21), (11),(19), and the momentum and state equation

$$\frac{\partial \rho}{\partial t} + \nabla\cdot(\rho\vec{\mathbf{u}}) = 0\ , \tag{28}$$

$$\epsilon\rho\frac{Du}{Dt} = -\frac{1}{\epsilon}\frac{\partial p}{\partial r}\ , \tag{29}$$

$$\rho\frac{Dw}{Dt} = -\frac{\partial p}{\partial z}\ , \tag{30}$$

$$\frac{\partial c}{\partial t} + \nabla\cdot(c\vec{\mathbf{u}}) = 0\ , \tag{31}$$

$$\frac{1}{\rho} = \frac{1-c}{\alpha} + c\ , \tag{32}$$

where α is the local gas density. Note that we have already applied the limit $Re \to \infty$ in this system, and in this limit, we need to ignore the no-slip boundary conditions along $r = 1$. Note, however, that (28)-(32) is underdetermined to solve for the set of unknowns u, w, p, c, ρ. To close this system, we need an additional relation between the pressure and the other set of unknows. For simplicity in the modeling, we consider

$$p = \rho = \frac{\alpha}{1 + (\alpha - 1)c}\ , \tag{33}$$

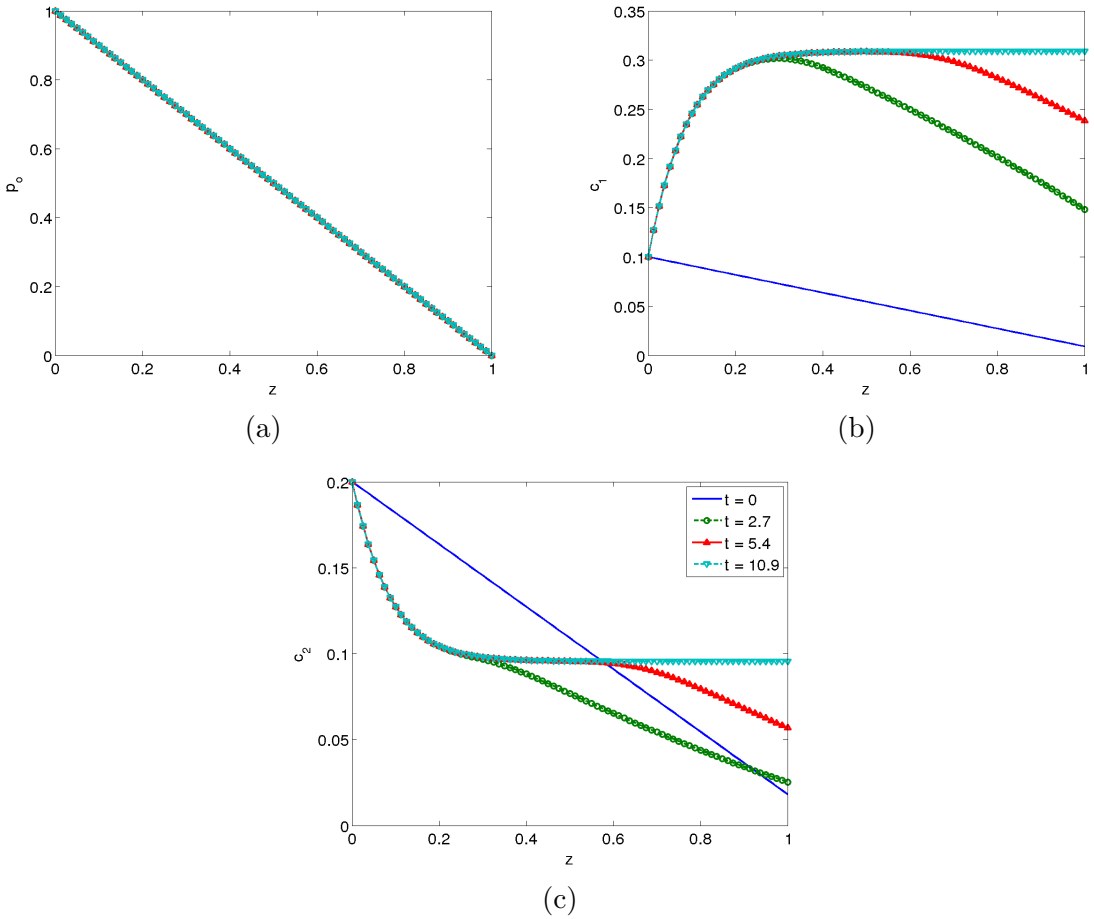

Figure 2: Typical simulation example with $\beta = 0.8, k = 1, M^2 = 0.001, c_{10} = 0.1, c_{20} = 0.2$, with 80 gridpoints in z and a time step $\Delta t = 0.025$.

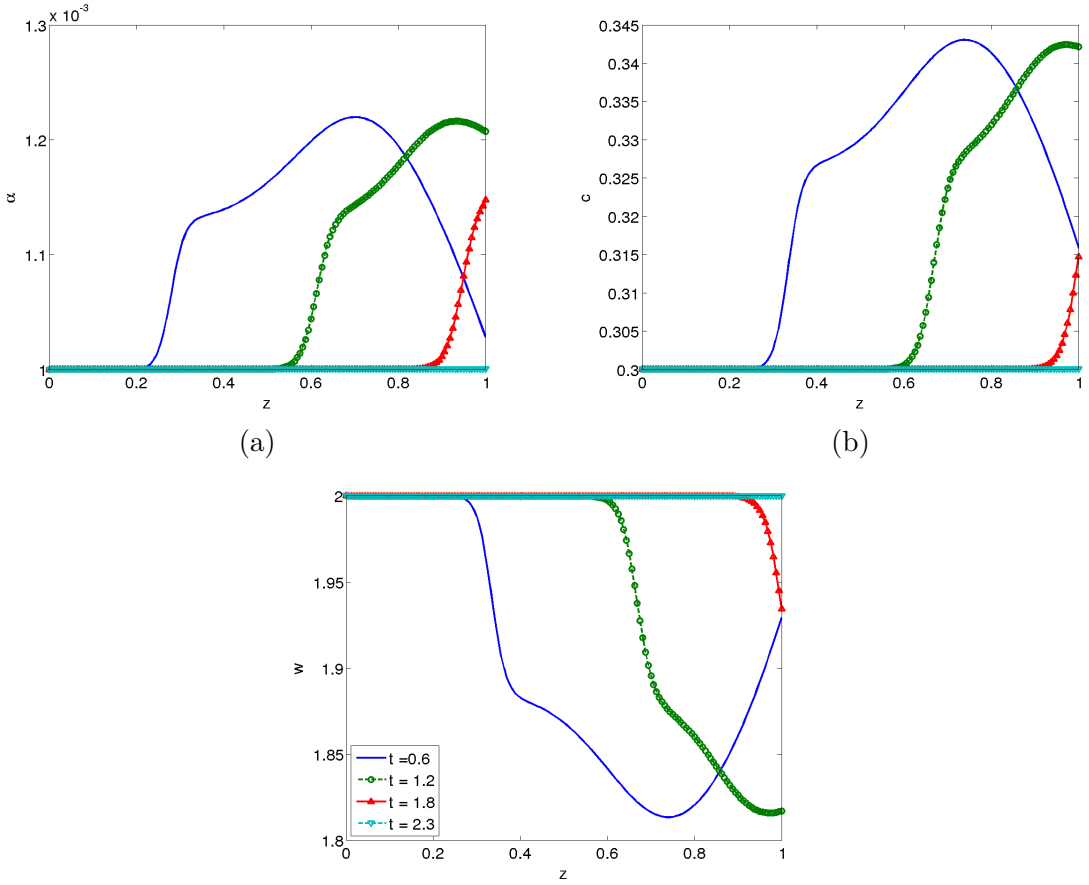

Figure 3: Typical simulation example with $\beta = 0.8, k = 1, M^2 = 0.001, c_{10} = 0.1, c_{20} = 0.2$, with 80 gridpoints in z and a time step $\Delta t = 0.025$.

which suggests that the pressure depends on the mixture density, and is a function of α and c.

The asymptotic approach is standard, and similar in its procedure to classical sheet equations [19]. Assuming that c_1, c_2 are independent of r, we find that the coupled set of equations to solve are of the form

$$\frac{\partial \rho}{\partial t} + \frac{\partial}{\partial z}(\rho w) = 0 \tag{34a}$$

$$\frac{\partial c_1}{\partial t} + \frac{\partial}{\partial z}(c_1 w) = 2\beta(kc_2 - c_1^2) \tag{34b}$$

$$\frac{\partial c_2}{\partial t} + \frac{\partial}{\partial z}(c_2 w) = -\beta(kc_2 - c_1^2) \tag{34c}$$

$$\frac{\partial w}{\partial t} + w\frac{\partial w}{\partial z} + \frac{1}{\rho}\frac{\partial \rho}{\partial z} = 0 \tag{34d}$$

with (32).

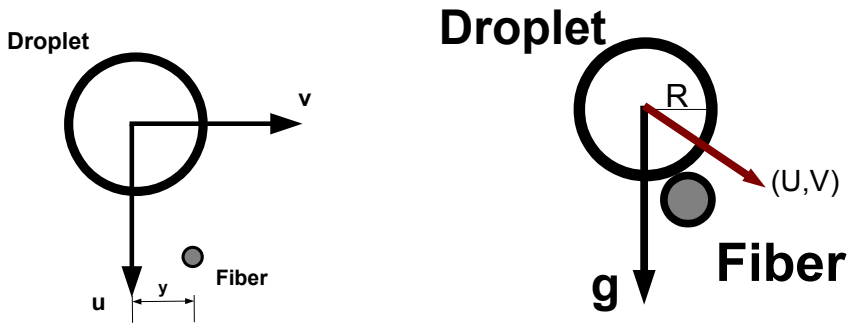

Figure 4: Schematic diagrams: (left) a spherical droplet approaching a cylindrical fiber, and (right) the droplet at the instant of first contact with the fiber.

3 Fiber-based droplet separators

At the macroscopic scale we considered models for the transport of droplets in the gas flow as locally-averaged densities taken over large collections of droplets. In a second approach, we considered a microscopic analysis of the separation of droplets as modeled by the collision of droplets with an individual fiber composing the filter.

Impingement separators [3] remove droplets from gas flows by passing the droplets through an array of obstacles. Droplets that hit an obstacle may coat its surface and will drain off to a collector in the form of a thin film flow. Packed-bed filters for removing particles from liquid flows work on a similar principle for removing the particles by attachment to the filter [9]. One form of impingement separator makes use of filter layers that are composed of arrays of either regularly spaced (wiremesh) or randomly arranged fibers. On a larger scale, the filter could be described as a porous media, but we will consider the fundamental situation of a single droplet hitting a solid cylinder, which can be then used as the basis for scaling up to describe the effectiveness of the overall filter by averaging over the array of fibers and the set of droplets. Some recent studies have examined the influence of flexibility of the fibers and droplets attaching to multiple fibers in the array [8].

3.1 A fluid droplet impacting a cylindrical fiber

As described earlier, large droplets are unstable and will fragment into numbers of small- to moderate-sized drops. These subsequent stable droplets will maintain approximately spherical shape as they move in the gas unless they collide with another droplet or a solid obstacle. While some other studies have used numerical simulations [10] to examine collisions with fibers, our work follows the model for the dynamics of the impact of a spherical droplet on a cylindrical fiber given in the 2004 paper of Lorenceau et al.[15]. The main issue to be understood is what conditions determine whether the impact causes the droplet to fragment [26, 28] (and produce smaller droplets that continue in the gas flow) or if the droplet will be captured by the fiber (and subsequent drains off).

Consider a droplet falling under the influence of gravity and hitting a horizontal circular cylinder. The mass for a droplet of radius R with density ρ is $m = \frac{4}{3}\pi R^3 \rho$. The radius of the fiber is b and

the x is oriented downward, in the direction of gravity, with the y-axis in the horizontal direction, see Fig. 4. The velocity of the droplet will be written as $\vec{\mathbf{u}} = (u, v)$ with components u, v in the x, y directions respectively.

3.1.1 Falling droplets

Before the droplet comes in contact with the fiber, the drop's motion will be governed by the acceleration due to gravity and the drop's interaction with the surrounding gas flow. The literature on raindrops includes some scientific disputes regarding the distribution of droplet sizes due to instabilities of large drops and details of fragmentation into smaller drops [22, 1, 24, 29]. We assume our droplets are below the typical size for fragmentation and remain spherical.

This regime can be described using models developed for falling rain drops [27],

$$m\frac{du}{dt} = -F_D + mg, \tag{35}$$

where F_D is the drag force on an object in a uniform surrounding flow of speed u, which takes the form

$$F_D = \tfrac{1}{2} C_D \rho u^2 A, \tag{36}$$

where A is the effective cross-sectional area of the object. Accounting for the relative velocity of the gas, U_g to the speed of the falling drop, equation (35) takes the form

$$\frac{du}{dt} = -\frac{3C_D}{8R}(u - U_g)^2 + g. \tag{37}$$

The solution of this equation for a droplet starting entrained with the gas flow at $t = t_0$, $u(t_0) = U_g$, is

$$u(t) = U_g + \sqrt{\frac{g}{\alpha}} \tanh\left(\sqrt{\alpha g}\,[t - t_0]\right), \tag{38}$$

where $\alpha = 3C_D/(8R)$. The corresponding vertical position for a droplet starting at $x(t_0) = x_0$ is then

$$x(t) = x_0 + U_g(t - t_0) + \frac{1}{\alpha} \ln\left(\cosh\left(\sqrt{\alpha g}\,[t - t_0]\right)\right). \tag{39}$$

Droplets falling over long distances will approach the equilibrium terminal velocity,

$$\bar{u}(R) = U_g + \sqrt{\frac{8gR}{3C_D}}. \tag{40}$$

Droplets that do not come in contact with a particular fiber are assumed to simply pass by without any interaction. Assuming the filter layer is sufficiently thick and the density of fibers is sufficiently high, most droplets should eventually impact on some fiber and (neglecting air currents or other drag effects) with speed on the order of (40).

3.1.2 Impact dynamics model

For droplets that do come in contact with fibers (see Fig. 4), we can write a force balance to describe the dynamics starting from the time after initial contact. First, consider the case of head-on collision with the fiber (as done in [15]), this means there is no lateral motion, $v = 0$ and the

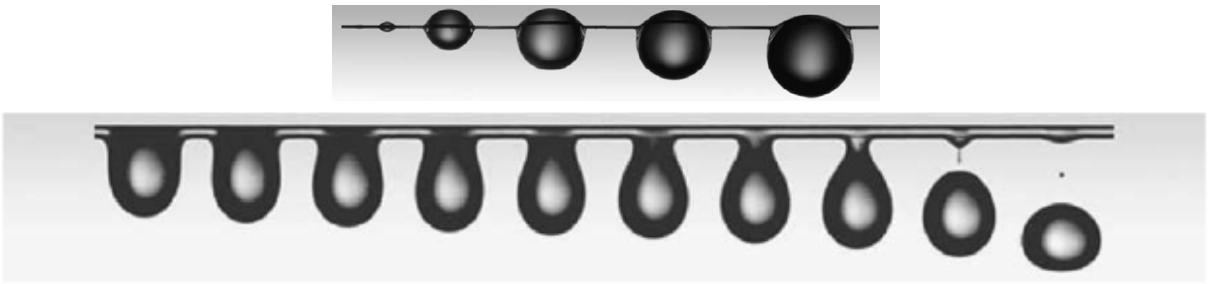

Figure 5: Photographs from [15]: (top) a series a stable, sessile (hanging) droplets on a horizontal fiber (all being below the critical size, $R < R_M$) and (bottom) a time-lapse series of images of a larger droplet, $R > R_M$, falling off a horizontal fiber.

drop is directly above the fiber, $y = 0$. Then Newton's second law can be written as

$$m\frac{du}{dt} = -F_D - F_C + mg, \tag{41}$$

where the F's represent two forces opposing the motion of droplet.

F_D is the drag force for a cylinder passing through a fluid and is taken to be of the form [15]

$$F_D = 4C_D\rho u^2 Rb, \tag{42}$$

where C_D is a drag coefficient constant for a cylinder, that can be expected to be near value one. This formula stems from the general expression for the drag on a rigid object due to a unbounded high velocity, low viscosity (low Reynolds number) surrounding fluid flow, $F_D = \frac{1}{2}C_D\rho u^2 A$ where A is the effective cross-sectional area of the object. However, the geometric factors in (42) do not directly correspond to a cross-sectional area. Here we have a drag due to the interaction with a finite volume of fluid. This form seems reasonable as it predicts a force that increases with increasing sizes of the fiber and droplet.

Similarly, while a full description of the effects of surface tension would require a direct numerical solution of the Navier Stokes equations, a rough estimate for an 'effective drag' due to surface tension is

$$F_C = 4\pi\gamma b, \tag{43}$$

where γ is the surface tension of the liquid. Consequently (41) becomes

$$\tfrac{4}{3}\pi R^3\rho\frac{du}{dt} = -4C_D\rho u^2 Rb - 4\pi\gamma b + \tfrac{4}{3}\pi R^3\rho g. \tag{44}$$

This equation can be nondimensionalized with respect to scales for droplet size and speed. A natural size scale is the maximum size for an equilibrium droplet hanging from a fiber [15], [4, 5, 18, 23, 17] (see Figure 5)

$$R_M = \left(\frac{3b\gamma}{\rho g}\right)^{1/3}, \tag{45}$$

which is set by a balance of gravity and surface tension; it can also be described as a ratio of the fiber radius to the capillary length scale, $\ell_c = \sqrt{\gamma/(\rho g)}$. Then a characteristic velocity scale [15] can be set as

$$U_M = \sqrt{4gR_M}. \tag{46}$$

Rescaling variables according to

$$u(t) = U_M \tilde{u}(\tilde{t}), \qquad R = R_M \tilde{r}, \qquad t = \frac{R_M}{U_M}\,\tilde{t}, \tag{47}$$

where $T_M = \sqrt{R_M/(4g)}$. Then (44) takes the form

$$\frac{d\tilde{u}}{d\tilde{t}} + \frac{\beta}{\tilde{r}^2}\tilde{u}^2 = \frac{1}{4} - \frac{1}{4\tilde{r}^3}, \tag{48}$$

where

$$\beta = \frac{3bC_D}{\pi R_M}. \tag{49}$$

Similarly to (38), the solution can be expressed in terms of a hyperbolic tangent, but instead of pursuing that form, we use the chain rule,

$$\frac{d\tilde{u}}{d\tilde{t}} = \frac{d\tilde{u}}{d\tilde{x}}\frac{d\tilde{x}}{d\tilde{t}} = \tilde{u}\frac{d\tilde{u}}{d\tilde{t}}, \tag{50}$$

to write (48) as an equation relating droplet mean velocity in terms of its spatial position relative to the fiber,

$$\frac{d(\tilde{u}^2)}{d\tilde{x}} + \frac{2\beta}{\tilde{r}^2}\tilde{u}^2 = \frac{1}{2} - \frac{1}{2\tilde{r}^3}, \tag{51}$$

where we pick the speed at first contact with the fiber to be $\tilde{u}_0$, setting the initial condition,

$$\tilde{u}(\tilde{x} = 0) = \tilde{u}_0. \tag{52}$$

Eqn (51) is a linear ODE that can be solved to yield

$$\tilde{u}^2(\tilde{x}) = \left(\frac{\tilde{r}^2}{4\beta} - \frac{1}{4\tilde{r}\beta}\right) + \left(\tilde{u}_0^2 - \frac{\tilde{r}^2}{4\beta} + \frac{1}{4\tilde{r}\beta}\right)\exp\left(-\frac{2\beta\tilde{x}}{\tilde{r}^2}\right). \tag{53}$$

This equation can only be valid for the range of positions describing the droplet being in contact with the fiber. If we assume that the droplet is large relative to the fiber radius, $R \gg b$, and that the droplet retains its spherical shape throughout the collision, then the range of contact should be $0 \le \tilde{x} \le 2$. Values in the range $\tilde{x} > 2$ imply that droplet has deformed and hence likely has fragmented into droplets or shed some mass onto the fiber, while its remaining mass continues in the gas flow. To describe successful capture of the droplet by the fiber, we require that droplet come to rest by the end of its range of motion,

$$\tilde{u}(\tilde{x}_*) = 0, \qquad 0 \le \tilde{x}_* \le 2, \tag{54}$$

where the upper bound $\tilde{x}_* = 2$ will correspond to the largest droplets. This yields a relation for the maximum entering speed for which capture can occur for a droplet of size $\tilde{r}$,

$$\tilde{u}_0^2 = \left(\frac{1}{\tilde{r}} - \tilde{r}^2\right)\left[\frac{e^{2\beta/\tilde{r}^2} - 1}{4\beta}\right]. \tag{55}$$

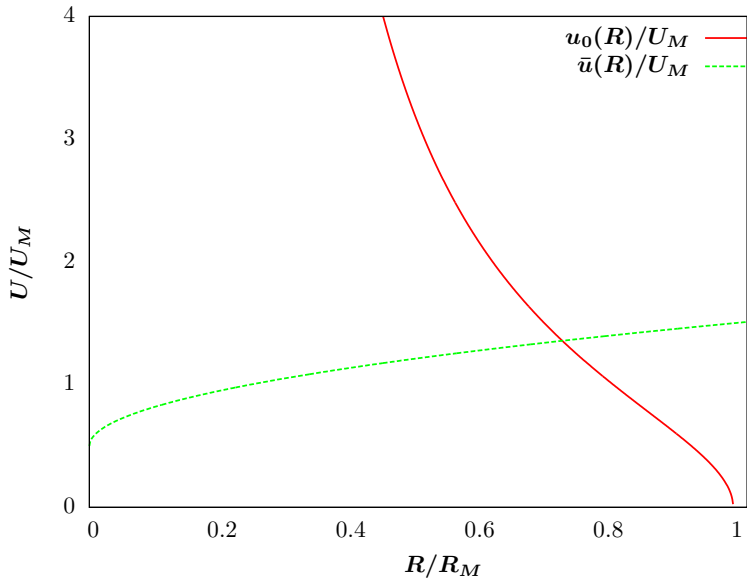

Figure 6: The scaled capture speed $u_0(R)$ (red curve) from (56) shown with the terminal velocity $\bar{u}(R)$ (green curve) with a gas speed of $U_g = 0.5U_M$ determining a reduced maximum capture-able droplet size of $R_M^* \approx 0.73R_M$.

Equation (55) is consistent with the fact that $R = R_M$ (45) is the size of the largest equilibrium droplets, since if $\tilde{r} = 1$ we get $\tilde{u}_0 = 0$ and there are no real-valued solutions for $\tilde{r} > 1$. Written in dimensional form, we get

$$u_0(R) = \sqrt{gR_M\left(\frac{R_M}{R} - \left[\frac{R}{R_M}\right]^2\right)\left(\frac{e^{2\beta R_M^2/R^2} - 1}{\beta}\right)}. \tag{56}$$

In [15], Lorenceau et al. showed that this relation matched well with experimental results.

We can equate (56) with the terminal velocity of falling droplets (40),

$$U_g + \sqrt{\frac{8gR}{3C_D}} = \sqrt{gR_M\left(\frac{R_M}{R} - \left[\frac{R}{R_M}\right]^2\right)\left(\frac{e^{2\beta R_M^2/R^2} - 1}{\beta}\right)},$$

which, for a given gas speed, $U_g \geq 0$, will determine a reduced value for the largest droplet that can be captured, $R_M^*(U_g) \leq R_M$, see Figure 6. Plugging in a drop radius of 100μm and a fiber radius of 10μm as well as the density of air and water we arrive at a gas velocity of approximately 3 meters per second.

Some work was done to try to generalize these impact dynamics to a two-dimensional dynamical system for $(u(t), v(t))$. Linear stability analysis for this system was carried out, but since the equilibrium obtained does not correspond to a captured state, it is not included here. Lorenceau et al. extended their model to describe off-centered impact of droplets on fibers in [16] and impacts on inclined fibers in [20].

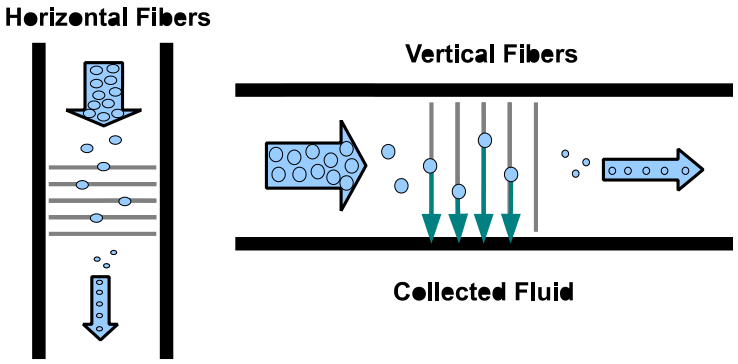

Figure 7: Schematic representations for (left) drops entrained in a vertical gas flow through an array of horizontal fibers and (right) horizontal motion of entrained drops impacting on vertical fibers.

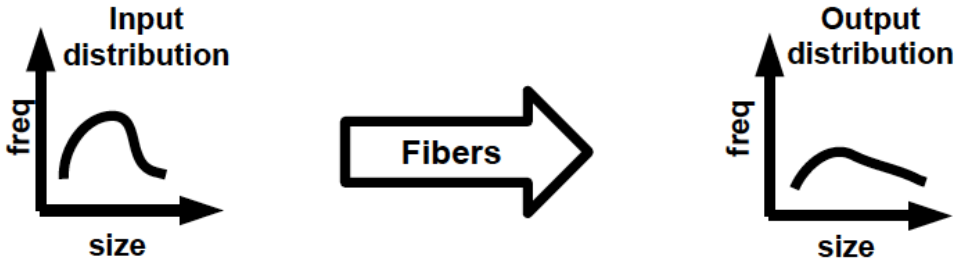

Figure 8: A schematic representation of the influence of the fibers in changing the distribution of droplets in the gas flow

3.1.3 Simulating drop distributions

In the previous subsection, we considered the case of vertical free-fall of drops onto a single horizontal fiber. A filter in a coalescer would have many many fibers in layers covering the entire cross-sectional area of the flow and could be oriented horizontally or vertically, see Figure 7. For the case of horizontal fibers, the captured sessile drops will slowly drain to collectors due to mutual coarsening interactions [2, 30] and boundary influences. Draining from vertical fibers will be a much faster process with transport driven by gravity. Draining can be described by thin film lubrication models [6] or by other physically-based models describing the motion of the droplets sliding down the fibers [11, 7]. Recent materials science studies of biologically-inspired designs for nonuniform fibers suggest that appropriate axial variations in fiber radius can significantly improve coalescence and draining [31, 25, 12].

In either case, the goal of the fiber filter is capture as many droplets as possible and remove them from the gas flow. Droplets that aren't captured by any of the fibers in the first layer of the filter may hit other fibers in layers deeper into the filter. Realistic gas flows will contain droplets having distributions of sizes and speeds and the overall effect of the fibers is to change these distributions by means of screening out the captured droplets, see Figure 8.

Using the model described in the previous section, we carried out some preliminary Monte

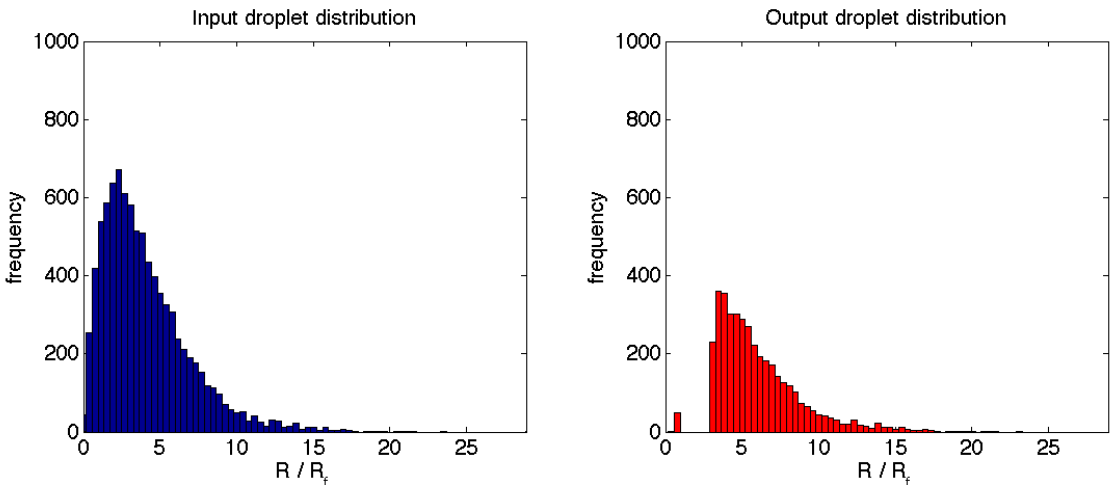

Figure 9: Input and output droplet size distributions for the droplet capture model with $u/U_M = 1$, $R/b = 2$. Here, due to the broad distribution of sizes, only small drops are captured and most drops pass through.

Carlo numerical simulations of large sets of droplets falling vertically through an array of identical horizontal fibers. The model is parametrized by a small number of physical properties:

1. R_M: the fiber radius relative to the capillary length scale, (45)
2. U_g/U_M: the gas flow speed relative to the characteristic speed, (46)
3. Geometric factors describing the spatial arrangement of the fiber array
4. Wetting material properties of the fiber surfaces
5. The distribution of droplet speeds relative to the average (assumed to be U_g)
6. The distribution of droplet sizes

In our first simulation the size distribution was taken to be a Gamma probability distribution, $\Gamma(2, 10)$, with probability density function $f(R) = cRe^{-R/10}$, used as a model of raindrop sizes [26, 27]. The results of the simulation are shown in Figure 9. As to be expected, given reasonable assumptions on fiber arrangement and draining, virtually all of the small ($R < R_M$) droplets were removed from the flow, but due to the form of the size distribution, the uncaptured larger droplets still comprised 80% of the original liquid content. Hence in this case, the filter was relatively ineffective.

In contrast, a second simulation considered droplets with the same speeds, and average size, but having a uniform distribution, see Figure 10. Using the same models for droplet capture and draining in the same layer of fibers, the output from this droplet distribution showed a dramatic decrease in liquid content of the filtered gas, down to 14% of the original level. While this comparison is not at all systematic, at a proof-of-concept level, it does show that the appropriate determination of fiber/filter parameters relative to the properties of the inflow droplet distribution can make very significant differences in the efficiency of the operation of the coalescer. Further work is needed to better understand how sensitive the output is to variations in the input parameters and how to map out the optimal filter design parameters.

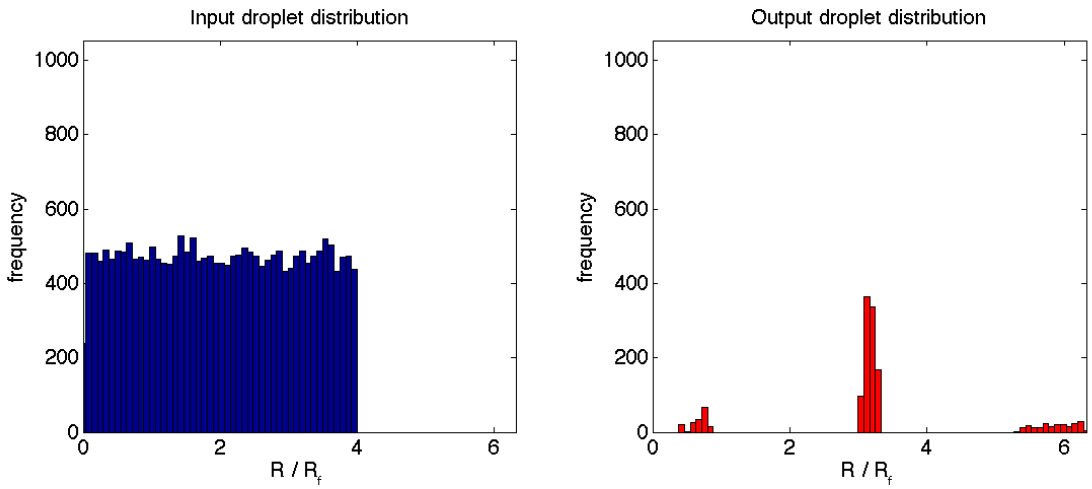

Figure 10: Input and output droplet size distributions for the droplet capture model with the same parameters, $u/U_M = 1$, $R/b = 2$. Here, the range of sizes covers only smaller drops, most are captured by the fiber filter.

4 Further work

In this report, we consider two different situations found in condenser and filtration applications. In Section 2, we assumed that the gas/droplet mixture can be described as a single component mixture (similar in spirit to that found in [14]). In this case, the steady-state pressures and liquid concentrations depend on how the density distribution of the mixture depends on concentration, fluid pressure, and other unknowns. This limitation is found for both small and large Reynolds numbers.

Secondly, we considered in Section 3 the velocity of a drop after impact with a cylindrical fiber. An ordinary differential equation describing this velocity is found, which includes the drag of the drop, cylinder and drop weight. A critical radius is found, as a function of the ambient gas velocity, below which droplets can be captured. However, the effectiveness of total fitration of fluid depends on the number density of the drops as a function of the drop radius.

Critical in both of these approaches is how the number density of the drop mixture relates to the gas velocity and pressure. Note that the number density can be expected to evolve over space and time, and how this interaction occurs depends on the momentum exchange between liquid and gas, which depends on capillarity. Future work on this problem requires that these dynamics are better understood.

References

[1] A. P. Barros, O. P. Prat, and F. Y. Testik. Size distribution of raindrops. *Nature Physics*, 6:232, 2010.

[2] B. J. Briscoe, K.P. Galvin, P.F. Luckham, and Saeid A.M. Droplet coalescence on fibres. *Colloids and Surfaces*, 56:301–312, 1991.

[3] A. Burkholz. *Droplet separation*. VCH publishing, New York, 1989.

[4] B. J. Carroll. The accurate measurement of contact angle, phase contact areas, drop volume, and Laplace excess pressure in drop-on-fiber systems. *Journal of Colloid and Interface Science*, 57(3):488–495, 1976.

[5] B. J. Carroll. The equilibrium of liquid drops on smooth and rough circular cylinders. *Journal of Colloid and Interface Science*, 97(1):195–200, 1984.

[6] R.V. Craster and O.K. Matar. On viscous beads flowing down a vertical fibre. *Journal of Fluid Mechanics*, 553:85–105, 2006.

[7] S. Dawar and G. G. Chase. Drag correlation for axial motion of drops on fibers. *Separation and Purification Technology*, 60:6–13, 2008.

[8] C. Duprat, S. Protiere, A. Y. Beebe, and H. A. Stone. Wetting of flexible fibre arrays. *Nature*, 482:510–513, 2012.

[9] M. Elimelech, J. Gregory, X. Xia, and R. A. Williams. *Particle deposition and aggregation.* Butterworth-Heinemann, Boston, 1998.

[10] J.M. Gac and L. Gradon. Analytical investigation and numerical modeling of collisions between a droplet and a fiber. *Journal of Colloid and Interface Science*, 369:419–425, 2012.

[11] T. Gilet, D. Terwagne, and Vandewalle N. Droplets sliding on fibres. *European Physical Journal E*, 31:253–262, 2010.

[12] Y. Hou, Y. Chen, Y. Xue, Y. Zheng, and L. Jiang. Water collection behavior and hanging ability of bioinspired fiber. *Langmuir*, 28:4737–4743, 2012.

[13] D.D. Joseph. Fluid dynamics of two miscible liquids with diffusion and gradient stresses. *Eur. J. Mech. B/Fluids*, 9:565–596, 1990.

[14] L. van Wijngaarden. One-dimensional flow of liquids containing small gas bubbles. *Annu. Rev. Fluid Mech.*, 4:369–396, 1972.

[15] E Lorenceau, C Clanet, and D Quere. Capturing drops with a thin fiber. *Journal of Colloid and Interface Science*, 279(1):192–197, 2004.

[16] E Lorenceau, C Clanet, D Quere, and M. Vignes-Adler. Off-centre impact on a horizontal fibre. *European Physical Journal-Special Topics*, 166:3–6, 2009.

[17] G. McHale, N. A. Kab, M. I. Newton, and S. M. Rowan. Wetting of a high-energy fiber surface. *Journal of Colloid and Interface Science*, 186:453–461, 1997.

[18] B. J. Mullins, I. E. Agranovski, R. D. Braddock, and C. M. Ho. Effect of fiber orientation on fiber wetting processes. *Journal of Colloid and Interface Science*, 269:449–458, 2004.

[19] A. Oron, S.H. Davis, and S.G. Bankoff. Long-scale evolution of thin liquid films. *Rev. Mod. Phys.*, 69(3):931–980, 1997.

[20] K. Piroird, C. Clanet, and D. Lorenceau, E.and Quere. Drops impacting inclined fibers. *Journal of Colloid and Interface Science*, 334:70–74, 2009.

[21] J. Qian and C. K. Law. Regimes of coalescence and separation in droplet collision. *Journal of Fluid Mechanics*, 331:59–80, 1997.

[22] E. Reyssat, F. Chevy, Biance A.-L., L. Patitjean, and D. Quere. Shape and instability of free-falling liquid globules. *European Physics Letters*, 80(34005):1–5, 2007.

[23] B. Song, A. Bismarck, R. Tahhan, and J. Springer. A generalized drop length – height method for determination of contact angle in drop-on-fiber systems. *Journal of Colloid and Interface Science*, 197:68–77, 1998.

[24] M. Szakall, S. K. Mitra, K. Diehl, and S. Borrmann. Shape oscillations of falling raindrops - a review. *Atmospheric Research*, 97:416–425, 2010.

[25] X. Tian, Y. Chen, Y. Zheng, H. Bai, and L. Jiang. Controlling water capture of bioinspired fibers with hump structures. *Advanced Materials*, 23:5486–5491, 2011.

[26] E. Villermaux. Fragmentation. *Annual Review of Fluid Mechanics*, 39:419–446, 2007.

[27] E. Villermaux and B. Bossa. Single-drop fragmentation determines size distribution of raindrops. *Nature Physics*, pages 697–702, 2009.

[28] E. Villermaux and B. Bossa. Drop fragmentation on impact. *Journal of Fluid Mechanics*, 668:412–435, 2011.

[29] E. Villermaux and F. Eloi. The distribution of raindrop speeds. *Geophysical Research Letters*, 38(L19805):1–4, 2011.

[30] A.L. Yarin, G.G. Chase, W. Liu, S.V. Doiphode, and D.H. Reneker. Liquid drop growth on a fiber. *AIChE Journal*, 52(1):217–226, 2006.

[31] Y. Zhang, H. Bai, Z. Huang, X. Tian, F-.Q. Nie, Y. Zhao, J. Zhai, and L. Jiang. Directional water collection on wetted spider silk. *Nature*, 463:640–643, 2010.